

AD-A181 452

AVALANCHING IN SINGLE-EVENT-UPSET CHARGE COLLECTION IN  
SEMICONDUCTOR DIODES(U) HARRY DIAMOND LABS ADELPHI MD  
A L WARD FEB 87 HDL-TR-2106

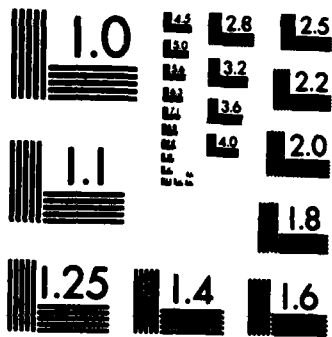
1/1

UNCLASSIFIED

F/G 9/1

ML





MICROCOPY RESOLUTION TEST CHART  
NATIONAL BUREAU OF STANDARDS-1963-A

The findings in this report are not to be construed as an official Department of the Army position unless so designated by other authorized documents.

Citation of manufacturers' or trade names does not constitute an official indorsement or approval of the use thereof.

Destroy this report when it is no longer needed. Do not return it to the originator.

AD A181 452

REPORT DOCUMENTATION PAGE				
1a. REPORT SECURITY CLASSIFICATION UNCLASSIFIED		1b. RESTRICTIVE MARKINGS		
2a. SECURITY CLASSIFICATION AUTHORITY		3. DISTRIBUTION / AVAILABILITY OF REPORT Approved for public release; distribution unlimited.		
2b. DECLASSIFICATION / DOWNGRADING SCHEDULE				
4. PERFORMING ORGANIZATION REPORT NUMBER(S) HDL-TR-2106		5. MONITORING ORGANIZATION REPORT NUMBER(S)		
6a. NAME OF PERFORMING ORGANIZATION Harry Diamond Laboratories	6b. OFFICE SYMBOL (if applicable) SLCHD-NW-RE	7a. NAME OF MONITORING ORGANIZATION		
6c. ADDRESS (City, State, and ZIP Code) 2800 Powder Mill Road Adelphi, MD 20783-1197		7b. ADDRESS (City, State, and ZIP Code)		
8a. NAME OF FUNDING / SPONSORING ORGANIZATION U.S. Army Laboratory Command	8b. OFFICE SYMBOL (if applicable)	9. PROCUREMENT INSTRUMENT IDENTIFICATION NUMBER		
8c. ADDRESS (City, State, and ZIP Code) 2800 Powder Mill Road Adelphi, MD 20783-1145		10. SOURCE OF FUNDING NUMBERS		
		PROGRAM ELEMENT NO. 6.21.20.A	PROJECT NO 1L162120 AH25	TASK NO. WORK UNIT ACCESSION NO.
11. TITLE (Include Security Classification) Avalanching in Single-Event-Upset Charge Collection in Semiconductor Diodes				
12. PERSONAL AUTHOR(S) Alford L. Ward				
13a. TYPE OF REPORT Final	13b. TIME COVERED FROM Oct 85 TO Jun 86	14. DATE OF REPORT (Year, Month, Day) February 1987	15. PAGE COUNT	
16. SUPPLEMENTARY NOTATION AMS code: 612120.H250011; HDL project: XE7625				
17. COSATI CODES			18. SUBJECT TERMS (Continue on reverse if necessary and identify by block number)	
FIELD	GROUP	SUB-GROUP	Avalanche, single-event upset, charge collection, semiconductor, silicon, gallium arsenide, carrier recombination	
09	03			
18	06			
19. ABSTRACT (Continue on reverse if necessary and identify by block number)				
<p>The one-dimensional computer program DIODE has been used to calculate charge collection in single ionizing events in silicon and gallium arsenide diodes. Avalanche multiplication is calculated to occur above a threshold of 3 V in a silicon diode, in agreement with published measurements. Since avalanching may lead to burnout in very-large-scale-integration semiconductors, it is a greater danger than the funneling effect of space charge. Carrier recombination is found to be important in gallium arsenide.</p>				
20. DISTRIBUTION / AVAILABILITY OF ABSTRACT <input checked="" type="checkbox"/> UNCLASSIFIED/UNLIMITED <input type="checkbox"/> SAME AS RPT. <input type="checkbox"/> DTIC USERS		21. ABSTRACT SECURITY CLASSIFICATION UNCLASSIFIED		
22a. NAME OF RESPONSIBLE INDIVIDUAL Alford L. Ward		22b. TELEPHONE (Include Area Code) (202) 394-3010	22c. OFFICE SYMBOL SLCHD-NW-RE	

## CONTENTS

	<u>Page</u>
SUMMARY .....	5
1. INTRODUCTION .....	7
2. APPROACH .....	7
3. RESULTS .....	7
3.1 Silicon .....	7
3.2 Gallium Arsenide .....	16
4. DISCUSSION .....	19
5. CONCLUSIONS .....	21
ACKNOWLEDGMENT .....	22
REFERENCES .....	22
DISTRIBUTION .....	23

## FIGURES

1. Current density as a function of time for track density of $1 \times 10^{14} \text{ cm}^{-3}$ .....	8
2. Avalanche oscillations for 20- $\mu\text{m}$ diode .....	8
3. Minimum avalanche and breakdown voltages .....	9
4. Current density as a function of time for track density of $1 \times 10^{18} \text{ cm}^{-3}$ .....	10
5. Charge multiple as a function of voltage .....	11
6. Carrier distributions at selected times .....	12
7. Electric field distributions at selected times .....	12
8. Current density as a function of time at selected diode widths .....	13
9. Current density as a function of time for 11-V applied voltage. ....	13
10. Maximum electric field as a function of time .....	14

FIGURES (cont'd)

	<u>Page</u>
11. Maximum electric fields for various track densities .....	14
12. Maximum electric fields for various diode widths .....	14
13. Comparison of Schottky and PN junction diodes .....	15
14. Current density as a function of time at various track densities .....	16
15. Time and current ratios as a function of diode width .....	16
16. Distance for time and current ratios as a function of track density .....	17
17. Carrier distributions for GaAs diode .....	18
18. Dielectric relaxation time and polarization distance .....	19
19. Two-dimensional field contours .....	20

TABLES

1. Electron Velocity Versus Field Parameters for GaAs used in Simulations 1 and 2 .....	17
--	----

### SUMMARY

Single-event upset of digital circuits due to an ionizing particle is a threat to an increasing portion of the Army's electronics. Extensive work in modeling this effect has been done at various laboratories. These modeling efforts have been focused on field funneling, and all have neglected avalanche multiplication, even though one experimental paper from the Naval Research Laboratory (NRL) has shown the importance of avalanching. This report verifies that importance by obtaining good agreement between our computer calculations and NRL measurements. Avalanching may lead to burnout in very high speed integrated circuits (VHSIC). The present calculations are one dimensional and need to be verified by two-dimensional calculations. This report is an expansion of another work.\*

---

\*Alford L. Ward, Avalanching in Single-Event-Upset Charge Collection in Semiconductor Diodes, IEEE Trans. Nucl. Sci., NS-33 (December 1986), pp 1552-1559.



Accession For	
NTIS CRA&I	<input checked="" type="checkbox"/>
DTIC TAB	<input type="checkbox"/>
U. announced	<input type="checkbox"/>
Justification	
By	
Distribution /	
Availability Codes	
Dist	Avail and/or Special
A-1	

## 1. INTRODUCTION

When a highly ionizing particle produces a track of dense ionization in a semiconductor and affects device operation through charge collection, a single-event upset is said to occur. There is now extensive literature [1]\* on this topic.

Campbell et al [2] have published measurements showing that avalanche multiplication is important in charge collection in single-event upsets. They noted evidence of avalanche multiplication above 3 V in a silicon diode which showed a breakdown voltage of about 7 V. Many papers (e.g., H. L. Grubin et al [3]) have reported numerical studies of charge collection from ionized-particle tracks, but none, to our knowledge, have included avalanche multiplication. The emphasis in most of these papers has been on the field funneling effect [4], a result of the extension of the high field region, which causes charge collection from beyond the normal depletion region of the device.

This paper presents our approach to the avalanche calculations, gives results of calculations of avalanche multiplication in silicon and gallium arsenide diodes, and concludes with further discussion and conclusions.

## 2. APPROACH

Charge collection of tracks from an ionizing particle has been calculated with the Harry Diamond Laboratories one-dimensional (1D) computer program DIODE. The computer program has been described previously [5]. Briefly, the continuity, current density formulation, and Poisson's equations are solved explicitly in their difference form. For these calculations, a constant voltage was applied through a series resistance of 50  $\Omega$  to the diode, which was shunted by a 1-pF capacitance. An area of  $1 \times 10^{-8}$  cm<sup>2</sup> was chosen for most calculations to determine the interaction of the diode with the external circuit. Ideal Schottky barrier diodes were simulated for all calculations except where a comparison is made with a PN junction diode.

Uniform and equal densities of electrons and holes over the track length were added to the equilibrium reverse-bias distributions as initial conditions for the calculations. Therefore, only the decreasing current portion of the pulse is calculated.

## 3. RESULTS

### 3.1 Silicon

Most of the material parameters for the silicon calculations were those given by Sze [6]. However, the important avalanche coefficients were taken from Van Overstraeten and DeMan [7]. The first calculations were made for a 20- $\mu$ m N-type diode doped to  $1 \times 10^{15}$  cm<sup>-3</sup>. Ideal abrupt (Schottky barrier) junctions were used for most calculations. The calculated breakdown voltage is 250 V, and the depletion width is 19  $\mu$ m at breakdown. A negative differential resistance (second breakdown) is calculated at 327 V.

\*References appear on p 22.

Calculations were made for an ionized track density of  $1 \times 10^{14} \text{ cm}^{-3}$  in order to eliminate appreciable space-charge distortion. The resulting current density, with and without avalanche multiplication, is plotted in figure 1 for an applied voltage of 200 V and a 20- $\mu\text{m}$  track length. For fully saturated velocities of  $1 \times 10^7 \text{ cm/s}$  and no diffusion, the current density would drop linearly from  $320 \text{ A/cm}^2$  to zero at 0.2 ns. Actually, the field drops to near zero at  $17.4 \mu\text{m}$ , and the hole velocity is not saturated over about half the diode width. The inset of figure 1 shows the electron and hole densities across the diode at selected times for the calculation without avalanching. It is seen that the hole "front" is less steep than the electron front, because of the higher hole velocity as the field increases to the left. Avalanche multiplication was noted down to 120 V, slightly less than one-half the avalanche breakdown voltage.

At voltages well above the avalanche breakdown voltage, avalanche [8] (or IMPATT) oscillations are noted. These oscillations are comparatively large for a track density of  $2 \times 10^{15} \text{ cm}^{-3}$ . Figure 2 shows the temporal growth or decay for track lengths of 10 and 20  $\mu\text{m}$ . It is seen that the shorter track length, with only one-half the initial charge of the longer

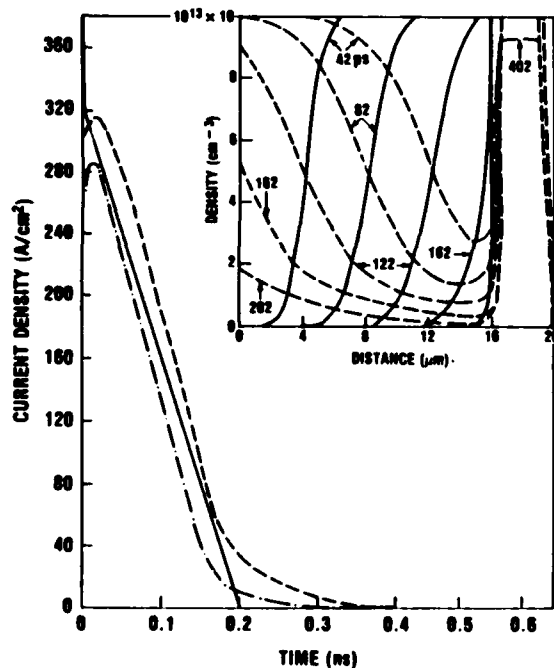


Figure 1. Calculated current density as a function of time for a track density of  $1 \times 10^{14} \text{ cm}^{-3}$  and a voltage of 200 V. Dashed curve includes avalanching, whereas dot-dashed curve does not. Inset shows electron (solid curves) and hole (dashed curves) density distributions for nonavalanching case at selected times in picoseconds.

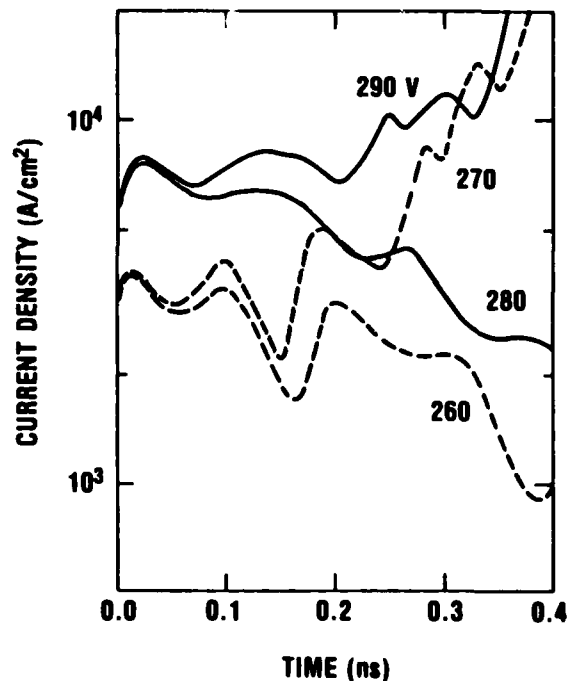


Figure 2. Computed avalanche oscillations are shown for a 20- $\mu\text{m}$  diode near the second breakdown voltage. Solid and dashed lines are for track lengths of 20 and 10  $\mu\text{m}$ , respectively. Initial track density is  $2 \times 10^{15} \text{ cm}^{-3}$ . Parameter is applied voltage.

track, has the lower second-breakdown voltage (current increasing indefinitely). This results from a more efficient avalanche oscillation; normally the second breakdown voltage decreases as the track density, as well as the total charge, increases.

The minimum voltage for avalanche multiplication,  $V_{\min}$ , and the second breakdown voltage,  $V_{B2}$ , are plotted as a function of track density in figure 3. Also plotted in this figure is the avalanche breakdown voltage,  $V_{B0}$ , for constant-doping, one-sided, N-type diodes as a function of that doping density. The latter calculations pertain to diodes not punched through at breakdown; diodes which punch through before breakdown have lower breakdown voltages. The criterion for  $V_{\min}$  was set at an increase of collected charge of about 5 to 10 percent; a more precise criterion would not be advantageous at this time. These calculations were made with various diode widths and track lengths equal to the diode width. For track densities of  $10^{16} \text{ cm}^{-3}$  and less, the diode width was  $20 \mu\text{m}$ ; for track densities of  $2 \times 10^{17} \text{ cm}^{-3}$  and greater, the diode width was  $1 \mu\text{m}$ . Intermediate diode widths were used, and overlapping track densities assured that there was little voltage variation with diode width for non-punched-through diodes. This figure is discussed further in section 4.

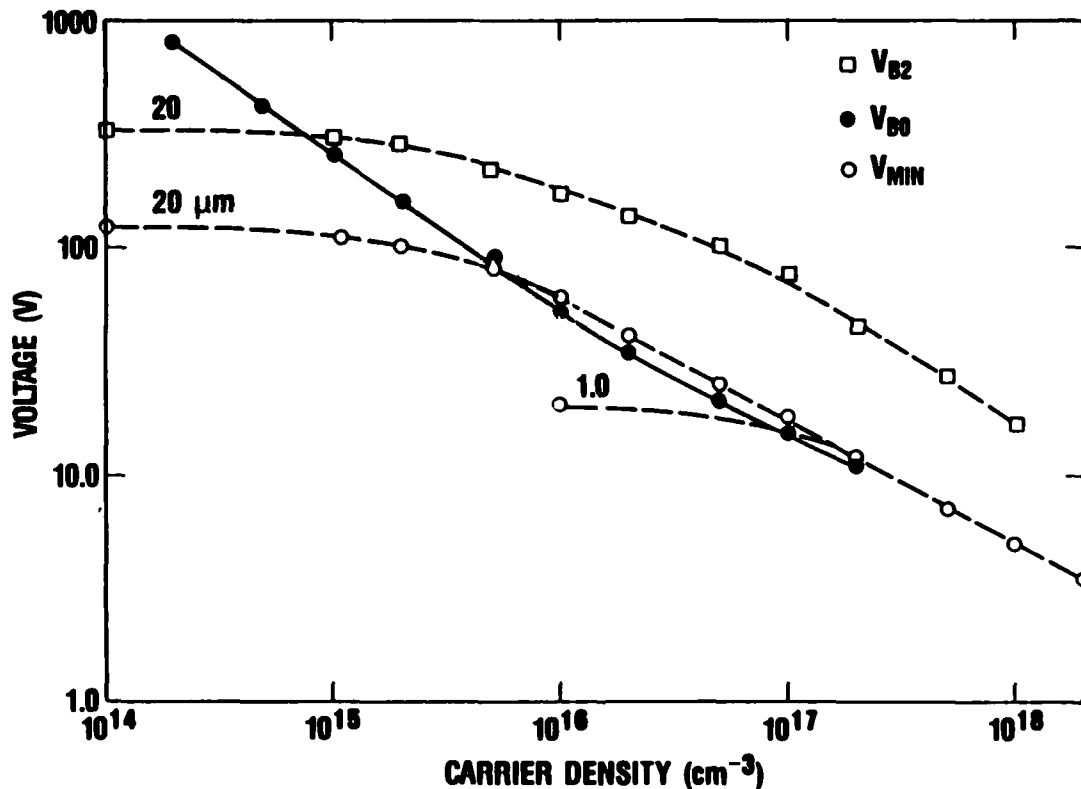


Figure 3. Minimum avalanche voltage ( $V_{\min}$ ) and second breakdown voltage ( $V_{B2}$ ) are plotted as a function of initial track densities. Parameter is diode width in micrometers. Also shown is first breakdown voltage ( $V_{B0}$ ) as a function of doping levels of N-type diodes.

Current density as a function of time is plotted in figure 4 for a 0.5- $\mu\text{m}$  P-type diode doped to  $1 \times 10^{15} \text{ cm}^{-3}$  an initial track density of  $1 \times 10^{18} \text{ cm}^{-3}$ , and various applied voltages. With neither space-charge effects nor diffusion, and assuming saturated velocities, the charge would be collected in 5 ps. At just above the minimum voltage for avalanche multiplication,  $V_{\text{min}} = 5 \text{ V}$ , the charge collection time is 32 ps. The charge collection time first decreases as the voltage increases and then increases as avalanche multiplication increases. The charge multiplier,  $M$ , the ratio of the total charge collected to the initial charge in the track, is shown in the inset of figure 4. The inset curve has the same shape as the measured curve of Campbell et al [2], namely, approximately an exponential increase from a constant value at low voltages. The measured curves were for similar doping, geometry, and track parameters as the calculations. Also plotted in the inset of figure 4 are the results for calculations for a 1- $\mu\text{m}$  diode.

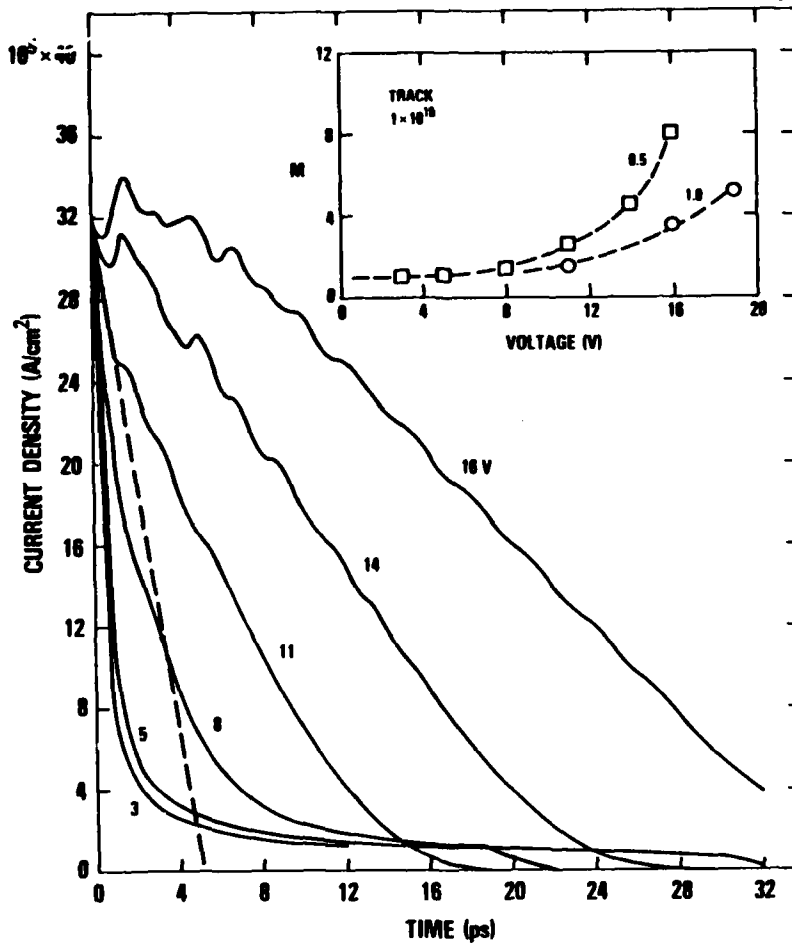


Figure 4. Current density as a function of time for a 0.5- $\mu\text{m}$  P-type diode doped to  $1 \times 10^{15} \text{ cm}^{-3}$ . Initial track density is  $1 \times 10^{18} \text{ cm}^{-3}$ . Parameter is applied voltage. Inset shows multiple of initial charge as a function of applied voltage for both the 0.5- $\mu\text{m}$  diode and a 1- $\mu\text{m}$  diode.

The inset curve data of figure 4 have been replotted in figure 5, where  $M - 1$  is plotted on a logarithmic scale against the voltage. Also plotted in this figure are the results for a  $0.2\text{-}\mu\text{m}$  diode with an initial track density of  $2 \times 10^{18} \text{ cm}^{-3}$  and for a  $0.1\text{-}\mu\text{m}$  diode with a density of  $5 \times 10^{18} \text{ cm}^{-3}$ . In order to plot the experimental data given in figure 2 of Campbell et al [2], in our figure 5, it is assumed that their charge collection efficiency (our multiplier  $M$ ) was equal to 1 at zero applied voltage. Their measured data are plotted in figure 5, with the further assumption that the built-in potential is 1 V. Last, calculated data for a track density of  $1 \times 10^{18} \text{ cm}^{-3}$  and a diode width of  $1 \mu\text{m}$  are also shown in figure 5 as the dashed curve. The point for  $V = 12 \text{ V}$  is estimated since mathematical calculation instability prevented a complete run. This is addressed in section 4. The measured data of Campbell et al [2] were taken with a diode with an epitaxial layer that was originally  $3 \mu\text{m}$ , but they estimate that the layer was reduced to  $1 \mu\text{m}$  by diffusion during the diode processing.

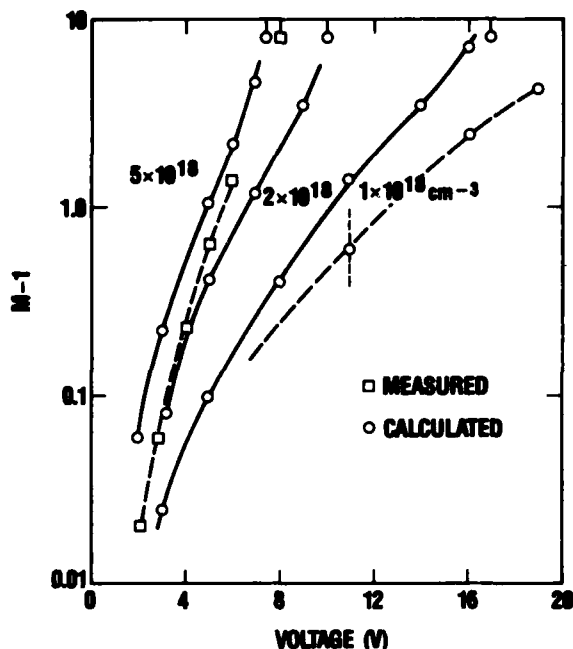


Figure 5. Charge multiple,  $M$ , less one is plotted on a logarithmic scale against applied voltage. Parameter for calculated curves is initial track density. Diode widths are given in text. Measured data are from Campbell et al [2]. Points at top of figure are second breakdown voltages.

The inset of figure 1 shows the electron and hole distributions across the diode during charge collection for small (mobile) space charge conditions. Figure 6 shows the calculated distributions of electrons and holes during charge collection in the P-type diode doped to  $1 \times 10^{15} \text{ cm}^{-3}$ . The initial track density is  $1 \times 10^{18} \text{ cm}^{-3}$  and the applied voltage is 3 V, about the avalanche threshold. Note the steepness of the concentration gradients as electrons move to the right and the holes to the left. The steepness results from the higher field and thereby higher velocity seen by the trailing carriers. The charge density "shoulders," especially noticeable from 1 to 4 ps (at densities from  $1 \times 10^{14}$  to  $3 \times 10^{16} \text{ cm}^{-3}$ ) are the result of avalanche multiplication. The fluctuation of carriers about the  $1 \times 10^{18} \text{ cm}^{-3}$  concentration (shown only for two curves) is not physical, but a result of incipient calculation instability. Increasing the number of calculation grid points removes the instability, which is discussed later.

The field distributions corresponding to the distributions in figure 6 are shown in figure 7. A logarithmic scale is used to show more detail. The high fields in the depleted regions are contrasted to the low fields in the

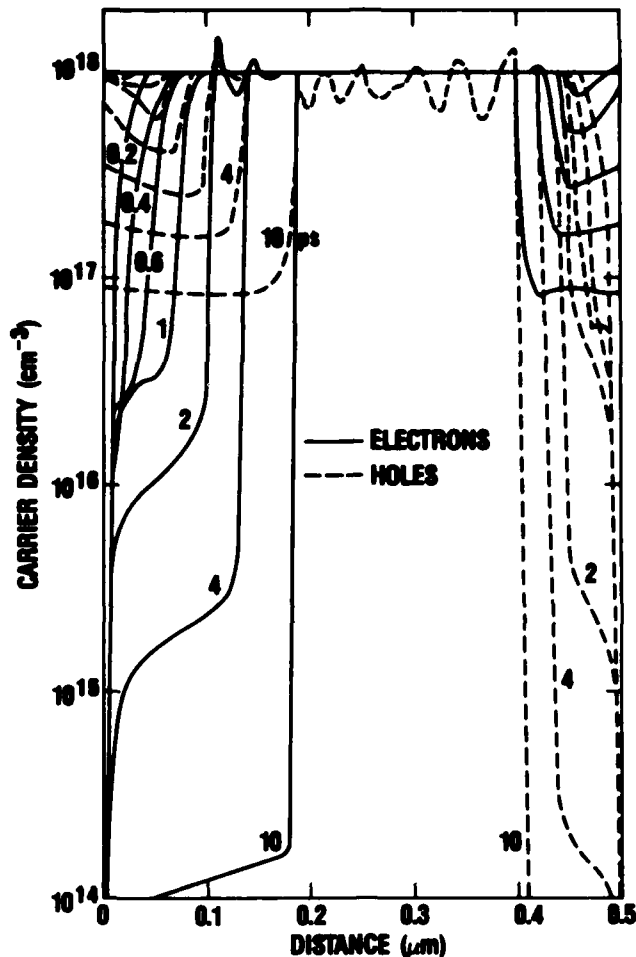


Figure 6. Carrier distributions at selected times are shown for a P-type diode doped to  $1 \times 10^{15} \text{ cm}^{-3}$ . Electron densities are shown by solid lines and hole distributions by dashed lines. Parameter is time in picoseconds.

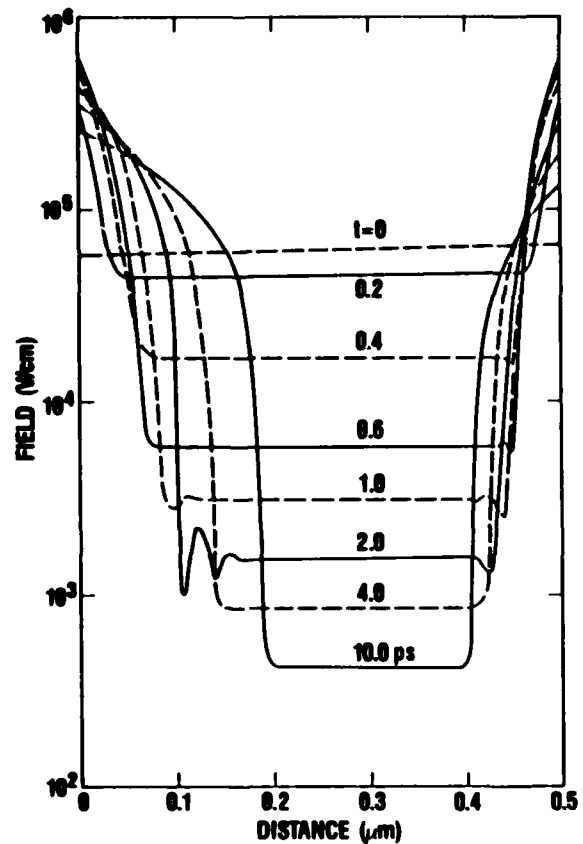


Figure 7. Electric field distribution corresponding to carrier distributions of figure 6. Parameter is time in picoseconds.

the plasma region. The maximum field is  $6 \times 10^5 \text{ V/cm}$  at 0.6 ps. This maximum field is for the avalanche threshold voltage. Higher fields are calculated at higher voltages. The time to attain the maximum field assumes zero time for track formation.

The current density as a function of time, corresponding to figures 6 and 7, was shown in figure 4 as a linear plot (the curve labeled 3 V). The same data are shown in figure 8 as a log-log plot (the curve labeled 1  $\mu\text{m}$ ). Also shown in this figure are results of calculations for diode widths of from 0.5 to 5  $\mu\text{m}$ . Calculations became unstable for the wider diodes at times from 1 to 10 ps. The temporal current decay for the same diodes is shown in figure 9 for an applied voltage of 11 V. Note that the curves for 0.5 and 1.0  $\mu\text{m}$  cross. The other curves would also cross if the calculations had not become unstable.

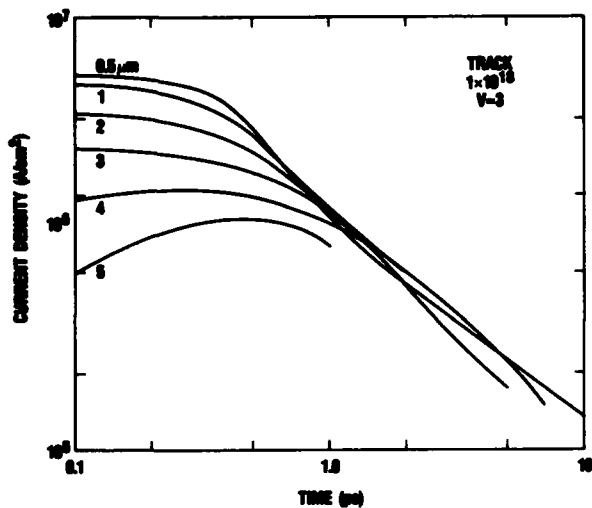


Figure 8. Current density plotted as a function of time on a log-log scale. Track density is  $1 \times 10^{18} \text{ cm}^{-3}$ , applied voltage is 3 V, and diode width in micrometers is given as parameter.

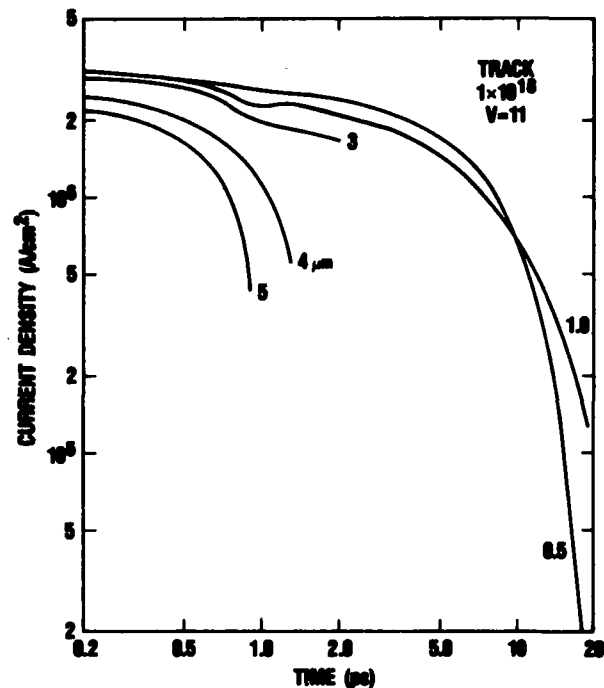


Figure 9. Current density as function of time for an applied voltage of 11 V.

The maximum field (usually at the cathode, but sometimes at the anode) is plotted as a function of time in figure 10. Again, a log-log plot is chosen and the data are for the 0.5- $\mu\text{m}$ -width diode. The effect of avalanche multiplication is in evidence (at the highest applied voltages). It is also seen that the peak of the maximum voltage occurs at later times for the higher voltages.

The maximum electric field as a function of time for various track densities is shown in figure 11. The diode widths for the diodes in order of decreasing track density were 1.0, 3.0, 15, and 20  $\mu\text{m}$ . The applied voltages were at the avalanche threshold and may be obtained from figure 3. The doping density for all diodes was  $1 \times 10^{15} \text{ cm}^{-3}$ .

The maximum field across the diode at any time is plotted in figure 12(a) as a function of diode width. The track density is  $1 \times 10^{18} \text{ cm}^{-3}$ , and the diode is doped to  $1 \times 10^{15} \text{ cm}^{-3}$ . For the higher applied voltages, calculations were made with and without avalanche multiplication. In these cases, higher fields occurred with avalanching than without. At lower track densities, avalanching reduced the maximum fields calculated. Figure 12(b) shows the maximum field at zero (and at infinite) times. Diodes below the dashed lines are punched through at the indicated voltage; that is, the field at the anode is zero.

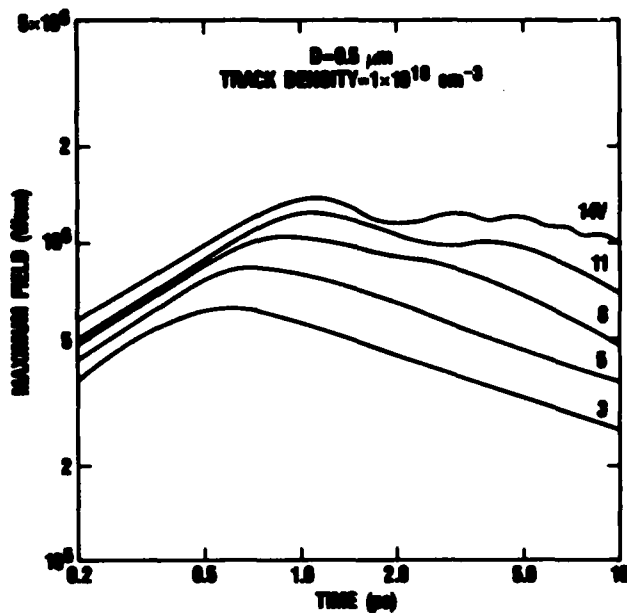


Figure 10. Maximum field as a function of time for a 0.5- $\mu\text{m}$  diode and a track density of  $1 \times 10^{18} \text{ cm}^{-3}$ ; parameter is the applied voltage.

As indicated earlier, most calculations have been made simulating ideal, abrupt, Schottky barrier diodes. Calculations were also made to simulate a PN junction diode: the width of the P region was  $0.1 \mu\text{m}$  and the N doping was  $1 \times 10^{15}$  for the  $1\text{-}\mu\text{m}$  diode. The initial track density was  $1 \times 10^{17} \text{ cm}^{-3}$ . The comparison of the two diodes with an applied voltage of 14 V showed that the current agreed to within 2 percent at all times. However the maximum calculated field was less for the junction diode, as shown in figure 13, where the field distributions are shown at selected times for the two diodes. The applied voltage is just above the avalanche threshold, and the charge multiplication is nearly equal for

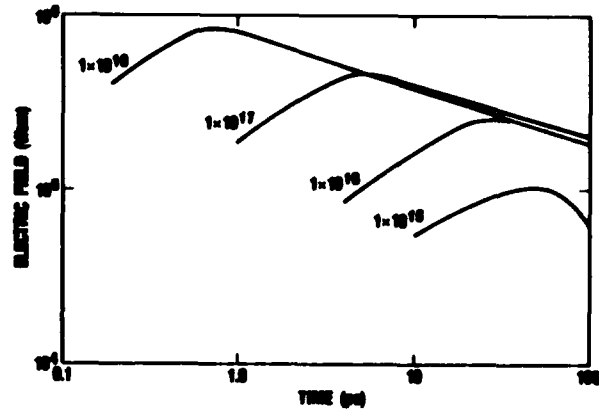


Figure 11. Maximum electric field as a function of time for various track densities ( $\text{cm}^{-3}$ ).

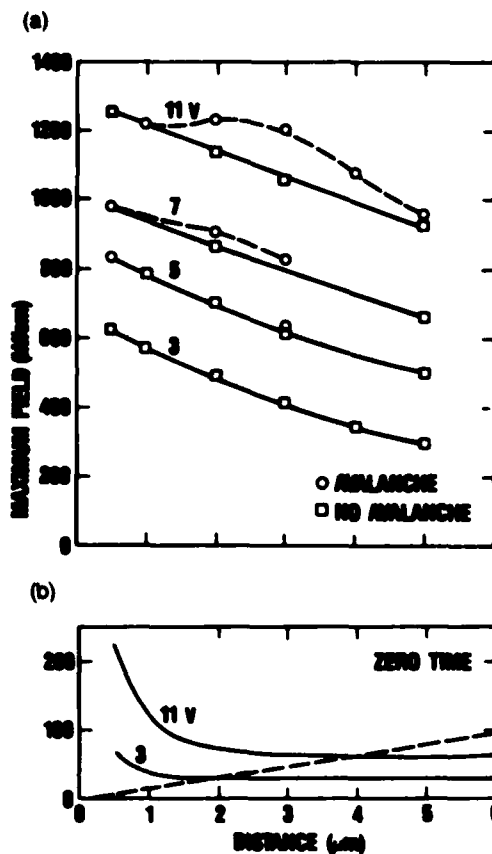


Figure 12. Maximum field (a) at any time given as a function of diode width and (b) at zero time. Diodes below the dashed line are punched through.

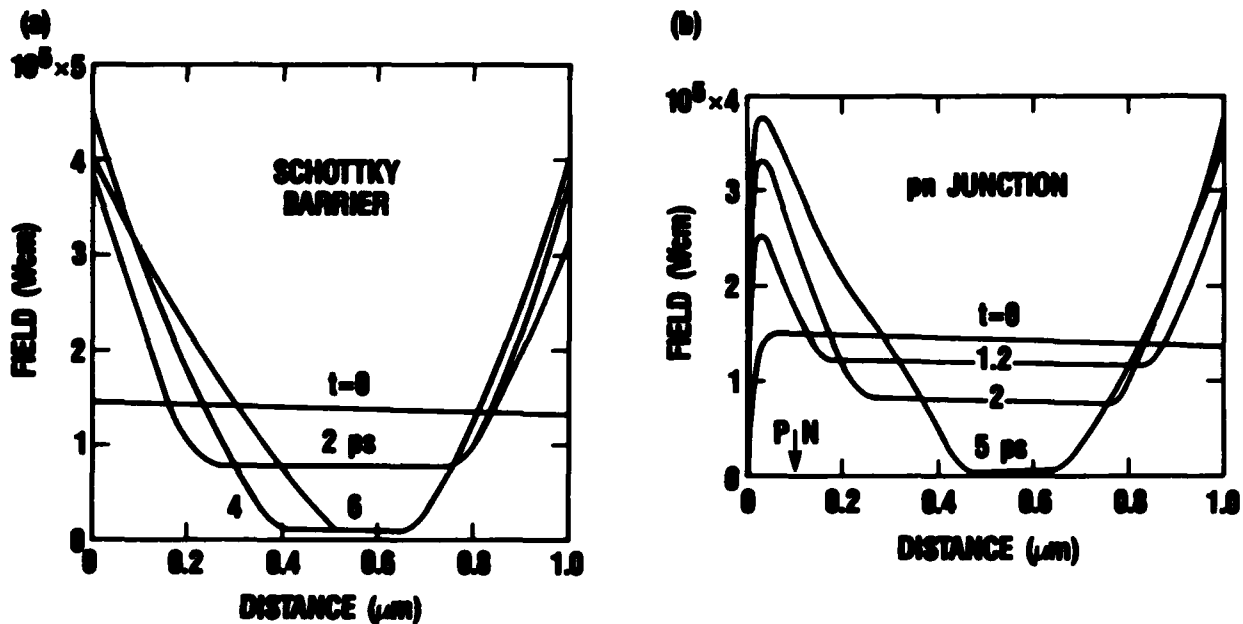


Figure 13. Comparison of field distributions for (a) a Schottky diode and (b) a PN junction diode. N-type diode is doped to  $1 \times 10^{15} \text{ cm}^{-3}$ , applied voltage is 14 V, and initial track density is  $1 \times 10^{17} \text{ cm}^{-3}$ . Parameter is time in picoseconds.

both diodes because, although the maximum field is less, the high field region is wider for the junction diode. Maximum fields are attained at 4 ps for the Schottky diode and at 5 ps for the junction diode.

Calculated current densities are plotted against time on a log-log scale in figure 14 for three initial track densities:  $1 \times 10^{16}$ ,  $1 \times 10^{17}$ , and  $1 \times 10^{18} \text{ cm}^{-3}$ . These diodes are doped to  $1 \times 10^{15} \text{ cm}^{-3}$  and the calculations are made at the avalanche threshold voltage, but with the avalanche coefficients equal to zero. Further calculations have been made for two and five times these track densities and for at least two diode widths. For clarity, two diode widths are shown only for the  $1 \times 10^{16} \text{ cm}^{-3}$  track density. The curves essentially coincide for the two diode widths until the charge is nearly completely removed in the shorter diode, when its current drops abruptly. The saturated-velocity transit time,  $T_0$ , for the 8- $\mu\text{m}$  diode is 80 ps, whereas the sharp-drop transition time,  $T_t$ , is 130 ps. Likewise,  $T_0 = 150$  ps and  $T_t = 700$  ps for the 15- $\mu\text{m}$  diode. When the time ratio  $T_t/T_0$  is plotted against diode width on a log-log plot, a straight line with a slope of 2 results for each track density; i.e.,  $T_t = T_0(d)d^2$ . This is shown in figure 15(a). Since  $T_0$  is proportional to  $d$ , the pulse collection time is proportional to  $d^3$ . In the same manner, a current density ratio may be defined by the ratio of the current at  $t = 0$  to the current at  $T_t$ . This current ratio increases quadratically with the diode width at each track density calculated, as shown in

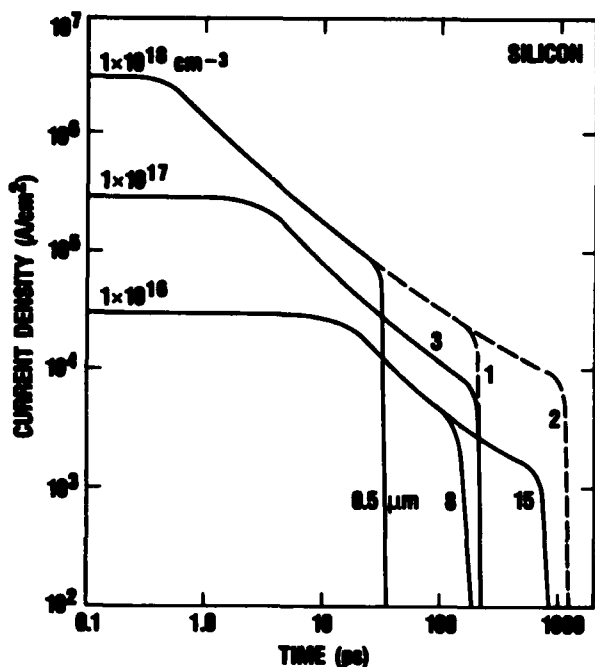


Figure 14. Calculated current density is plotted as a function of time for diodes doped to  $1 \times 10^{15} \text{ cm}^{-2}$ . Diode widths in micrometers are given on right of figure, whereas initial track densities in  $\text{cm}^{-3}$  are given on left. Dashed curves are extrapolated.

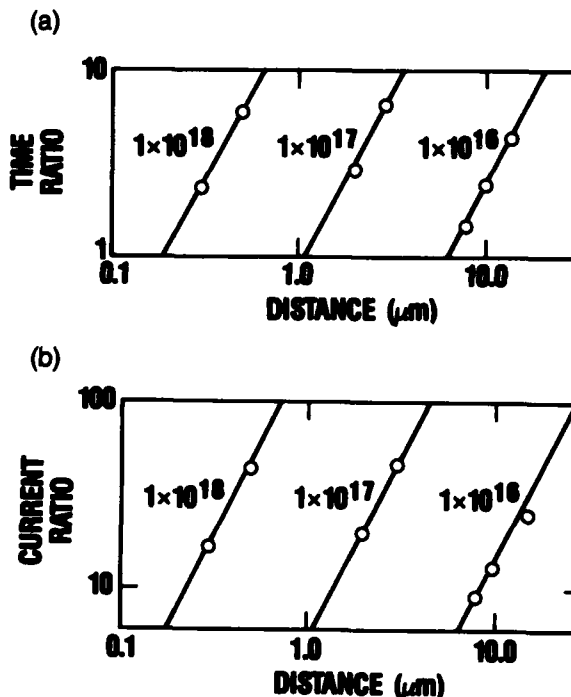


Figure 15. Log-log plot of time and current ratios (defined in text) as a function of diode widths. Parameter is initial track density in  $\text{cm}^{-3}$ .

figure 15(b). These extrapolation expressions were used to construct the current-density-versus-time curves for an initial track density of  $1 \times 10^{18} \text{ cm}^{-3}$  and diodes widths of 1 and 2  $\mu\text{m}$ , as shown by the dashed curves of figure 14. The dashed curves were replotted on a linear scale, and the total charge collected was obtained graphically. In each case the total charge was found to be equal to the initial charge in the track.

The distance corresponding to the time ratio,  $T_t/T_0 = 4$  (an average value was chosen), is plotted in figure 16 on a log-log plot as a function of track density. A straight line of the slope  $-0.75$  is shown. Likewise, a similar plot for a fixed current ratio has the same slope. These extrapolations were found to be useful in estimating collection times for calculations made with track densities higher than  $1 \times 10^{18} \text{ cm}^{-3}$ .

### 3.2 Gallium Arsenide

The material parameters of gallium arsenide are not as well known as those of silicon. The ionization coefficients were chosen to give a reasonable fit to the data of Bulman et al [9]. Two electron-velocity-versus-field curves were used. The parameters are listed in table 1. The hole mobility was chosen as  $400 \text{ cm}^2/\text{V-s}$ , and the saturation velocity of  $1 \times 10^7 \text{ cm/s}$  attained at a field of  $5 \times 10^4 \text{ V/cm}$ . The other material parameters were taken from Sze [6].

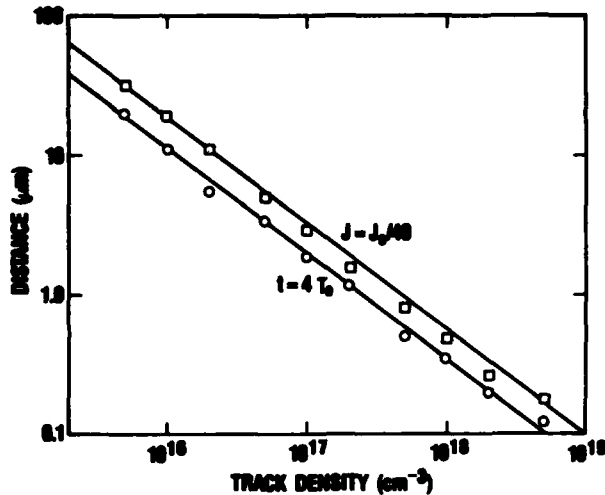


Figure 16. Distance required for  $T = 4T_0$  and for  $J = J_0/40$  is plotted against track density.

TABLE 1. ELECTRON VELOCITY VERSUS FIELD PARAMETERS FOR GaAs USED IN SIMULATIONS 1 AND 2

Parameter	Simulation 1	Simulation 2	Units
Low field mobility	7000	8500	$\text{cm}^2/\text{V}\cdot\text{s}$
Maximum velocity	$1.9 \times 10^7$	$2.1 \times 10^7$	cm/s
Field at maximum velocity	$5.8 \times 10^3$	$5.0 \times 10^3$	V/cm
Minimum velocity	$6.8 \times 10^6$	$6.0 \times 10^6$	cm/s
Field at minimum velocity	$5.0 \times 10^4$	$1.3 \times 10^5$	V/cm
Saturated velocity	$1 \times 10^7$	$1 \times 10^7$	cm/s

The avalanche breakdown voltage for a 20- $\mu\text{m}$  GaAs diode doped to  $1 \times 10^{15} \text{ cm}^{-3}$  was found to be 295 V, compared to 250 V in silicon. Calculations have been made for only two track densities,  $1 \times 10^{14} \text{ cm}^{-3}$  and  $1 \times 10^{18} \text{ cm}^{-3}$ . The collection currents as a function of time were quite similar to those for silicon in each case. These current curves were also nearly the same for the two electron-velocity-versus-field curves, although the electron distributions at fixed times were greatly changed. Figure 17(a) shows the distribution of carriers at selected times for a 20- $\mu\text{m}$  P-type GaAs diode doped to  $1 \times 10^{15} \text{ cm}^{-3}$ . The track density is  $1 \times 10^{14} \text{ cm}^{-3}$ , the voltage is 260 V, and the ionization coefficients were set to zero. The electron and hole velocities are plotted as a function of distance in figure 17(b).

For the P-type diode the field is low, and the electron velocity is high on the cathode (left) side of the figure. The higher velocity of the trailing electrons causes the peaking of the electron distribution at the

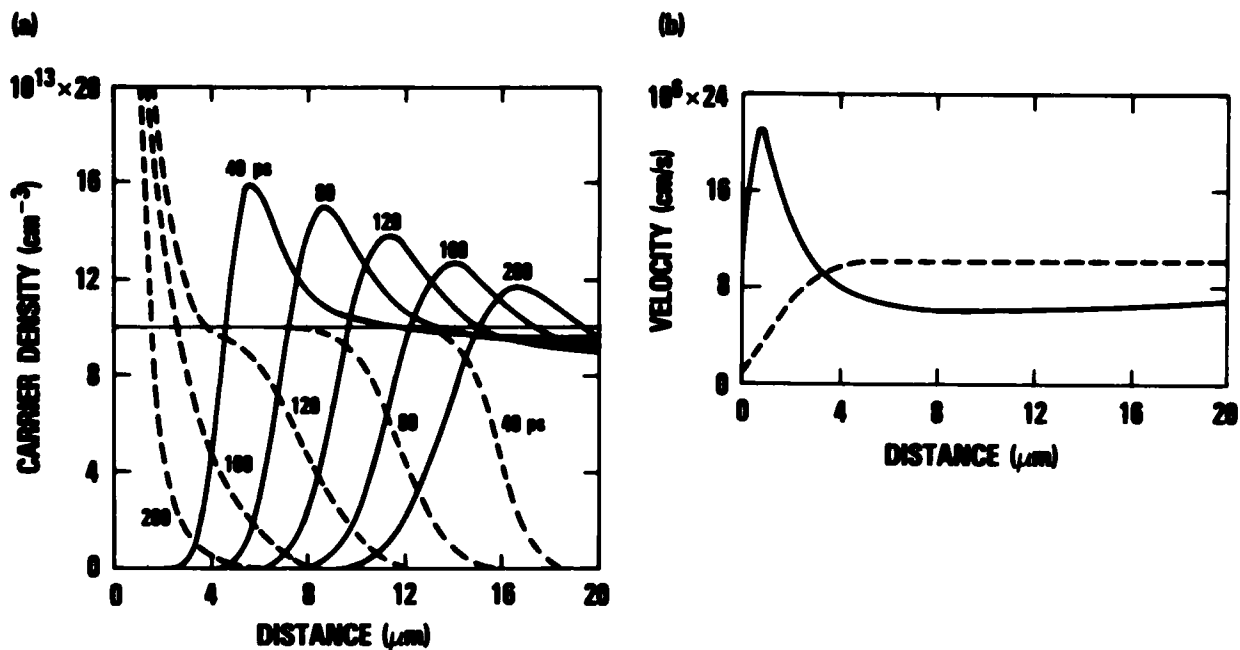


Figure 17. (a) Carrier distribution at selected times in picoseconds for P-type GaAs diode doped to  $1 \times 10^{15} \text{ cm}^{-3}$ . Electron distributions are shown as solid curves while hole distributions are dashed. (b) Electron (solid) and hole (dashed) velocities are given as a function of position.

trailing edge. The velocity of the trailing edge of the electron distribution (specifically the  $5 \times 10^{13} \text{ cm}^{-3}$  location) is found to be  $6 \times 10^6 \text{ cm/s}$ , the input valley velocity. The holes accumulate near the cathode because their velocity is low there. For the complementary N-type diode, the high electron velocity region is near the anode, and a depletion of electrons develops there. Despite the marked differences in the carrier distributions between the P- and N-type diodes, the maximum difference in current density at any time is 3 percent. For the  $2 \times 10^{18} \text{ cm}^{-3}$  track density, the most noticeable effect of the negative-velocity-versus-field characteristic is that the field is essentially forbidden to be in the range for a negative velocity characteristic, with abrupt transitions in both time and space. Again, there is very little effect on the current density at any time.

The recombination lifetime in GaAs is not known even in order of magnitude. Sze [6] gives a lifetime,  $\tau_R$ , of  $\sim 10^{-8} \text{ s}$ . In the computer program DIODE the effective lifetime is inversely proportional to the carrier density. Calculations have been made in GaAs with infinite lifetime, with  $\tau_R = 10^{-8} \text{ s}$  and with  $\tau_R = 2 \times 10^{-9} \text{ s}$  for  $N = 1 \times 10^{15} \text{ cm}^{-3}$ . For the track density  $1 \times 10^{18} \text{ cm}^{-3}$  calculations, the infinite lifetime calculations showed collection currents closely agreeing with those of silicon. For the  $\tau = 2 \times 10^{-9} \text{ s}$  calculations, the total charge collected and the time for that collection were reduced by approximately one-half. This recombination effect is larger than that observed experimentally, but avalanching could reduce the charge loss due to recombination. The calculations indicate that the chief practical difference in charge collection between silicon and GaAs is that the latter has a higher recombination rate, reducing the collected charge.

#### 4. DISCUSSION

The most important question to be discussed is why our calculations show avalanche multiplication to be important, whereas other calculations [10] do not. One consideration is the grid spacing for calculations. In figure 7 it may be seen that at the time of the peak electric field the entire high field region is about 0.05- $\mu\text{m}$  wide. Certainly the grid spacing must be small compared to this distance. Kreskovsky and Grubin [10] used 28 unequally spaced grid points for their three-dimensional calculations for a 5- $\mu\text{m}$  silicon diode. Their densest spacing seems to be about 0.05  $\mu\text{m}$ . The maximum fields that Kreskovsky and Grubin [10] calculated were below the avalanche threshold, and they did not make avalanche calculations.

The DIODE computer program uses explicit difference equations, and for computational stability the time step must be less than the dielectric relaxation time,  $\tau_D = \epsilon/\sigma$ , where  $\epsilon$  is the dielectric constant and  $\sigma$  is the conductivity. This is actually a physical constraint for accurate space charge calculations. Further, the grid spacing must be small compared to the van Roosbroeck [11] polarization distance,  $X_p = (v_p + v_n)\tau_D$ , where  $v_p$  and  $v_n$  are the hole and electron velocities, respectively. When a normal distribution of minority carriers is injected into a semiconductor, majority carriers largely neutralize the space charge in small multiples of  $\tau_D$ , but the majority carrier distribution is dragged along behind the minority carrier distribution at a distance  $X_p$ .

For a track density of  $1 \times 10^{18} \text{ cm}^{-3}$  in silicon,  $\tau_D = 3 \times 10^{-15} \text{ s}$  and  $X_p = 6 \times 10^{-8} \text{ cm}$  for saturation velocities of  $1 \times 10^7 \text{ cm/s}$ . The calculations in figure 6 were actually made with a timestep of  $5 \times 10^{-15} \text{ s}$  and a grid distance of  $2 \times 10^{-7} \text{ cm}$ . A partial, but recoverable, instability is responsible for the fluctuations noted in figure 6. If either the time or distance step is doubled, irrecoverable instability results. A plot comparing successful and failed runs is shown in figure 18. The time step and the distance step used in each run are plotted as individual points against the track density in the figure. The straight lines are the pertinent dielectric relaxation times and polarization distance as a function of carrier density. Calculations made at lower track densities have shown that the temporal current decay is unaffected by the recoverable instability. Using these time and distance steps in a two- or three-dimensional (2D or 3D) calculation will be quite costly.

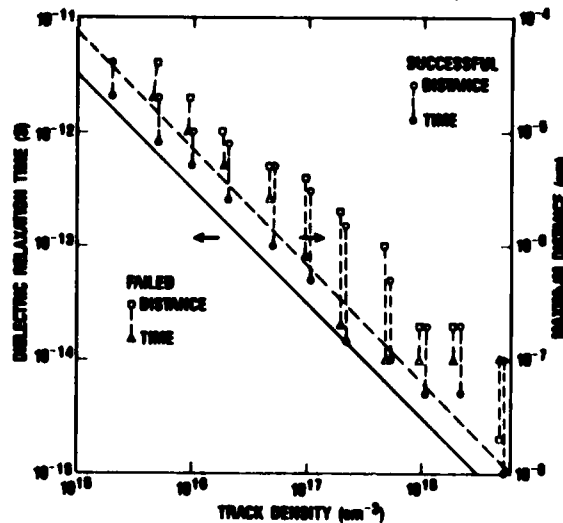


Figure 18. Dielectric relaxation time (solid line) and polarization distance (dashed line) are shown as a function of carrier density. Individual points are time and distance steps which resulted in successful or failed computer runs.

Some indication of the 2D aspect of charge collection can be deduced from 1D calculations. Figure 19(a) shows the field distribution calculated at 42 ps for a track density of  $2 \times 10^{15} \text{ cm}^{-3}$  in a 20- $\mu\text{m}$  N-type diode doped to  $1 \times 10^{15} \text{ cm}^{-3}$ . The applied voltage is 240 V and the avalanche constants were set to zero. Electrons are depleted from the first 4  $\mu\text{m}$ , increasing the field gradient, and holes from the last 2  $\mu\text{m}$ , reversing the field gradient. The latter is an example of field funneling. Figure 19(b) shows a sketch of constant field contours deduced from figure 19(a). The vertical axis (not quantified) is the track radius with the track centered. The field contours at the edges are equidistant, given by the field gradient at  $t = 0$ . The field at the center of the track is determined by the 42-ps curve of figure 19(a). The full contour is drawn freehand from the center to the end points. Current paths will follow the field lines, which are perpendicular to the field contours. Thus, the electrons will diverge from the track in the first 3  $\mu\text{m}$  and last 6  $\mu\text{m}$  from the cathode, and converge in between. For this example the maximum field at the cathode was 390 kV/cm; the maximum was reduced to 310 kV/cm for calculations including avalanche multiplication. Some calculations at a track density of  $1 \times 10^{18} \text{ cm}^{-3}$  show higher fields with avalanche than those without.

Diffusion in one and two dimensions can also be used to obtain some estimate of the error of 1D as compared with 2D calculations. The peak density of 2D diffusion from a line source decays at the same rate as the 1D diffusion from a plane source with double the diffusion constant. From this analogy and from the consideration of the previous paragraph, an estimate is made that the 2D calculation would have a maximum field of about one-half that calculated for the 1D calculation. In this context our 1D calculation would have about the same avalanche threshold and charge multiplier as would be obtained in a 2D calculation with double the track density. When it is considered that the track cross-sectional area may be unknown by an order of magnitude, the 1D calculation seems tolerable.

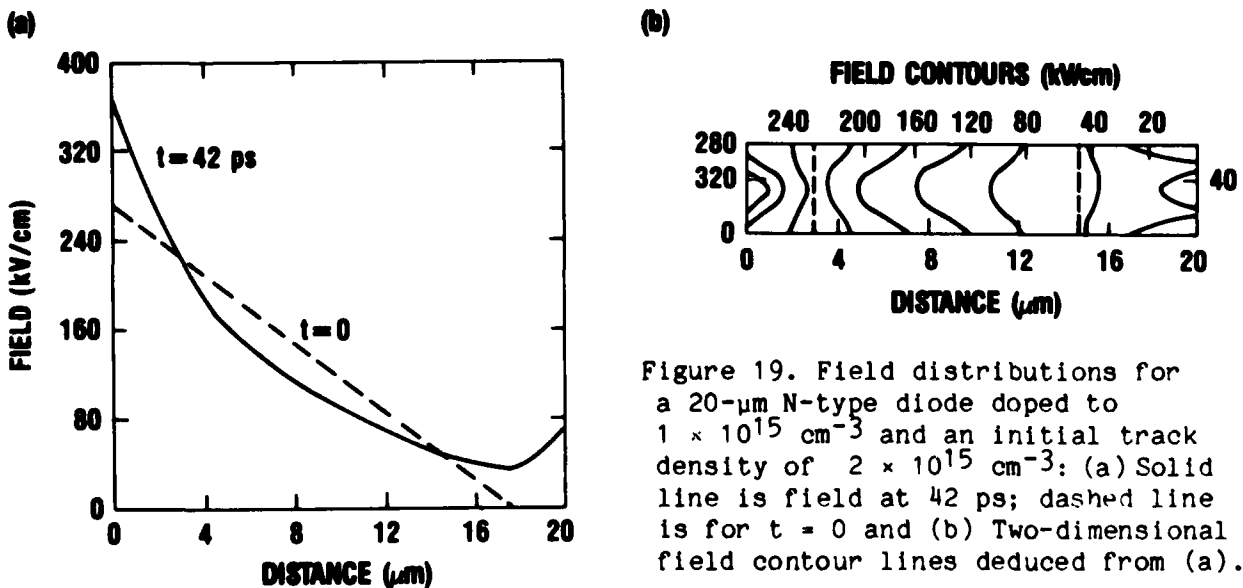


Figure 19. Field distributions for a 20- $\mu\text{m}$  N-type diode doped to  $1 \times 10^{15} \text{ cm}^{-3}$  and an initial track density of  $2 \times 10^{15} \text{ cm}^{-3}$ : (a) Solid line is field at 42 ps; dashed line is for  $t = 0$  and (b) Two-dimensional field contour lines deduced from (a).

Figure 3 shows close agreement between  $V_{min}$ , the minimum voltage for avalanche multiplication as a function of track density, and  $V_{B0}$ , the avalanche breakdown of one-sided diodes as a function of doping density, for carrier densities above  $10^{16} \text{ cm}^{-3}$ . The deviation below this density is due to the device width of  $20 \text{ } \mu\text{m}$  for the track calculation. This agreement may be understood from two considerations. First, in the one-sided diodes, avalanche multiplication is noted at about one-half of  $V_{B0}$ . Second, the high field region near the cathode is almost identical in the two calculations, since depletion is essentially complete in each case. However, in the track calculation, there is also a high field region near the anode due to hole depletion (see fig. 7). Therefore, the total voltage is nearly the same in each case.

It was shown in figure 7 that the maximum field was obtained in less than  $1 \text{ ps}$ . This time is comparable to the time for the ionizing particle to completely form the track. Therefore, an accurate calculation should include the formation of the track with the velocity of the ionizing particle.

The mobilities used in the calculations were characteristic of the  $10^{15} \text{ cm}^{-3}$  doping level rather than the usually higher track density. This assumption has the effect of increasing the current and thus reducing the time scale of the current pulse. However, carriers were at a saturated velocity for the most part, and saturated velocities are independent of carrier density.

The closeness of the agreement between the 1D calculation result and the measured data shown in figure 5 was unexpected. Various compensating errors may account for this. Campbell et al [2] estimate their diode width as  $1 \text{ } \mu\text{m}$ , but their breakdown voltage was about  $7 \text{ V}$ . Our calculations show that a  $1\text{-}\mu\text{m}$  diode should have a breakdown voltage at about  $35 \text{ V}$ . Although calculated breakdown voltages often exceed measured ones for various reasons, one suspects that their diode is no more than  $0.5 \text{ } \mu\text{m}$ . If this were so, their charge collection efficiency would be  $\sim 1.0$  instead of  $\sim 0.5$ , as they give for zero applied voltage. This was assumed in our figure 5. Our calculations assume that the ionized track was fully formed at zero time, but as seen in the previous paragraph, the maximum field was obtained in a time comparable to the transit time of the ionizing particle. Therefore, the high field at the anode due to depletion of holes would be delayed, and more voltage would be available for avalanche multiplication near the cathode. This possible factor of two field enhancement would negate the postulated factor of two decrease due to the 1D calculations.

## 5. CONCLUSIONS

One-dimensional calculations show that avalanche multiplication must be considered in the charge collection in single ionizing events. The calculated increase in charge multiplication as a function of voltage is shown to be in good agreement with the measurements of Campbell et al [2]. Charge multiplication becomes more important as the epitaxial layer decreases in thickness. Since one hardening technique is to reduce field funneling by using thinner epitaxial layers, one must beware of increasing the charge mul-

tiplication by a large factor due to avalanching while avoiding a limited multiplication due to funneling.

#### ACKNOWLEDGMENT

The author would like to express his appreciation to F. B. McLean for many useful discussions.

#### REFERENCES

- (1) Z. Shanfield, M. M. Moriwaki, W. M. Digby, J. R. Srour, and D. E. Campbell, Characteristics of SEU Current Transients and Collected Charge in GaAs and Si Devices, IEEE Trans. Nucl. Sci., NS-32 (December 1985), pp 4104-4109. Also other papers in the December issues of 1983-1985.
- (2) A. B. Campbell, A. R. Knudson, P. Shapiro, D. O. Patterson, and L. E. Seiberling, Charge Collection in Test Structures, IEEE Trans. Nucl. Sci., NS-30 (December 1983), pp 4486-4492.
- (3) H. L. Grubin, J. P. Kreskovsky, and B. C. Weinburg, Numerical Studies of Charge Collection and Funneling in Silicon Devices, IEEE Trans. Nucl. Sci., NS-31 (December 1984), pp 1161-1166.
- (4) C. M. Hsieh, P. C. Murley, and R. R. O'Brien, A Field-Funneling Effect in the Collection of Alpha-Particle-Generated Carriers in Silicon Devices, IEEE Elect. Device Lett., EDL-2 (April 1981), pp 103-105.
- (5) A. L. Ward, An Electro-Thermal Model of Second Breakdown, IEEE Trans. Nucl. Sci., NS-23 (December 1976), pp 1679-1684.
- (6) S. M. Sze, Physics of Semiconductor Devices, New York, John Wiley and Sons (1981).
- (7) R. Van Overstraeten and H. DeMan, Measurement of the Ionization Rates in Diffused Silicon P-N Junctions, Solid-State Electron., 13 (1970), pp 583-608.
- (8) A. L. Ward, Modes of Avalanche Oscillations in Silicon Diodes, IEEE Trans. Electron Devices, ED-25 (June 1978), pp 683-687.
- (9) G. E. Bulman, V. M. Robbins, K. F. Brennan, K. Hess, and G. E. Stillman, Experimental Determination of Impact Ionization Coefficients in (100) GaAs, IEEE Elect. Device Lett., EDL-4 (June 1983), pp 181-185.
- (10) J. P. Kreskovsky and H. L. Grubin, Numerical Simulation of Charge Collection in Two- and Three-Dimensional Silicon Diodes--A Comparison, Solid-State Electron., 29 (May 1986), pp 505-516.
- (11) W. van Roosbroeck, Current-Carrier Transport with Space Charge in Semiconductors, Phys. Rev., 123 (July 1961), pp 474-490.

## DISTRIBUTION

ADMINISTRATOR  
DEFENSE TECHNICAL INFORMATION CENTER  
ATTN DTIC-DDA (12)  
CAMERON STATION, BUILDING 5  
ALEXANDRIA, VA 22304-6145

COMMANDER  
US ARMY ARMAMENT, MUNITIONS, &  
CHEMICAL COMMAND  
ATTN DRSMC-LEP-L, TECHNICAL LIBRARY  
ATTN DRSMC-ASF, FUZE & MUNITIONS  
SUPPORT DIV  
ROCK ISLAND, IL 61299

DIRECTOR  
US ARMY BALLISTIC RESEARCH LABORATORY  
ATTN DRDAR-TSB-S (STINFO)  
ABERDEEN PROVING GROUND, MD 21005

US ARMY ELECTRONICS TECHNOLOGY  
& DEVICES LABORATORY  
ATTN DELET-DD  
FT MONMOUTH, NJ 07703

DIRECTOR  
US ARMY MATERIEL SYSTEMS ANALYSIS  
ACTIVITY  
ATTN DRXSY-MP  
ABERDEEN PROVING GROUND, MD 21005

COMMANDER  
US ARMY MISSILE & MUNITIONS  
CENTER & SCHOOL  
ATTN ATSK-CTD-F  
REDSTONE ARSENAL, AL 35809

US ARMY MOBILITY EQUIPMENT RESEARCH &  
DEVELOPMENT COMMAND  
ATTN DRDME-E  
ATTN DRDME-EC (2 COPIES)  
ATTN DRDME-EA (2 COPIES)  
ATTN DRDME-EM (2 COPIES)  
ATTN DRDME-EE (2 COPIES)  
ATTN DRCPM-MEP-D (2 COPIES)  
ATTN DRCPM-MEP-M (2 COPIES)  
ATTN DRCPM-MEP-T (2 COPIES)  
ATTN ATZA-TSM-G (2 COPIES)  
FT BELVOIR, VA 22060

NAVAL RESEARCH LABORATORY  
ATTN DR. ELIGIUS WOLICKI, CODE 6610  
ATTN DR. EDWARD PETERSON, CODE 6611  
ATTN A. R. KNUDSEN  
ATTN A. B. CAMPBELL  
WASHINGTON, DC 20375

HQ, USAF/SAMI  
WASHINGTON, DC 20330

DEPT OF THE AIR FORCE, HQ  
6585TH TEST GROUP (AFSC)  
RADAR TARGET SCATTER FACILITY  
ATTN LT COL RONALD L. KERCHER, CHIEF  
HOLLOMAN AFB, NM 88330

RELIABILITY ANALYSIS CENTER  
RADC (RBRAC)  
ATTN DATA COORDINATOR/GOVT PROGRAMS  
GRIFFISS AFB, NY 13441

ANALYTICAL SYSTEMS ENGINEERING CORP  
OLD CONCORD ROAD  
ATTN LIBRARIAN  
BURLINGTON, MA 01803

AT&T BELL LABORATORY  
ROOM 4M424  
ATTN DENIS LONGO  
CRAWFORDS CORNER ROAD  
HOLMDEL, NJ 07733

BOEING MILITARY AIRPLANE COMPANY  
ATTN CLETUS SUTTER  
M/S: K75-50  
3801 SOUTH OLIVER  
WICHITA, KS 67210

COMBAT DATA INFORMATION CENTER  
AFWL/FIESD (CDIC)  
WRIGHT PATTERSON AFB, OH 45433

ENGINEERING SOCIETIES LIBRARY  
ATTN ACQUISITIONS DEPARTMENT  
345 EAST 47TH STREET  
NEW YORK, NY 10017

IIT RESEARCH INSTITUTE  
ATTN AJAY K. BUTI  
10 W 35TH STREET  
CHICAGO, IL 60616

IRT CORPORATION  
ATTN J. C. PICKEL  
101 S KRAEMER BLVD, SUITE 132  
PLACENTA, CA 92670

JET PROPULSION LABORATORIES  
CALIFORNIA INSTITUTE OF TECHNOLOGY  
ATTN J. A. ZOUTENDYK  
4800 OAK GROVE DRIVE  
MAILSTOP 158-205  
PASADENA, CA 91109

MISSION RESEARCH CORPORATION  
CAPITOL BUILDING II, SUITE 201  
ATTN DR. BRUCE GOPLEN  
5503 CHEROKEE AVENUE  
ALEXANDRIA, VA 22312

DISTRIBUTION (cont'd)

NORTH CAROLINA STATE UNIVERSITY  
PO BOX 7911  
ATTN PROF SHERRA DIEHL  
RALEIGH, NC 27695-7911

NORTHROP CORPORATION  
RESEARCH & TECHNOLOGY CENTER  
ATTN DR. JOSEPH SROUR  
ONE RESEARCH PARK  
PALO VERDES PENINSULA, CA 90274

NORTHROP CORPORATION  
HYDRAULICS DESIGN ANALYSIS &  
TEST UNIT  
2301 WEST 120TH STREET  
HAWTHORNE, CA 90250

POLYTECHNIC INSTITUTE OF NEW YORK  
ROUTE 110  
ATTN PROF. ERIC E. KUNHARDT  
FARMINGDALE, NY 11735

SCIENTIFIC RESEARCH ASSOCIATION  
PO BOX 498  
ATTN HAROLD L. GRUBIN  
GLASTONBURY, CT 06033

TRW ATTN MARK A. HOPKINS  
ONE SPACE PARK  
REDONDO BEACH, CA 90278

US ARMY LABORATORY COMMAND  
ATTN COMMANDER, AMSLC-CG  
ATTN TECHNICAL DIRECTOR, AMSLC-CT

INSTALLATION SUPPORT ACTIVITY  
ATTN RECORD COPY, SLCIS-IM-TS  
ATTN LIBRARY, SLCIS-IM-TL (3 COPIES)  
ATTN LIBRARY, SLCIS-IM-TL (WOODBIDGE)  
ATTN TECHNICAL REPORTS BRANCH,  
SLCIS-IM-TR (2 COPIES)  
ATTN LEGAL OFFICE, SLCIS-CC

HARRY DIAMOND LABORATORIES  
ATTN D/DIVISION DIRECTORS  
ATTN DIVISION DIRECTOR, SLCHD-RT  
ATTN CHIEF, SLCHD-NW-E  
ATTN CHIEF, SLCDH-NW-EB  
ATTN CHIEF, SLCDH-NW-EC  
ATTN CHIEF, SLCDH-NW-ED  
ATTN CHIEF, SLCHD-NW-EE  
ATTN CHIEF, SLCHD-NW-R  
ATTN CHIEF, SLCHD-NW-RA  
ATTN CHIEF, SLCHD-NW-RC  
ATTN CHIEF, SLCHD-NW-RE  
ATTN CHIEF, SLCHD-NW-RH  
ATTN CHIEF, SLCHD-NW-RI  
ATTN CHIEF, SLCHD-NW-P  
ATTN F. McLEAN, SLCHD-IT-EB  
ATTN K. W. BENNETT, SLCHD-NW-RC  
ATTN T. OLDHAM, SLCHD-NW-RC  
ATTN R. GARVER, SLCHD-NW-RE  
ATTN R. GILBERT SLCHD-NW-RH  
ATTN A. WARD, SLCHD-NW-RE (10 COPIES)

ENO

7-87

Ditic